Green's function method for elimination of the spurious multipole interaction in the surface/interface slab model

Ikutaro Hamada,[1,*] Minoru Otani,[2] Osamu Sugino,[3] and Yoshitada Morikawa[4,2]
[1]*WPI-Advanced Institute for Materials Research, Tohoku University, 2-1-1 Katahira, Aoba-ku, Sendai 980-8577, Japan*
[2]*Research Institute for Computational Sciences (RICS), National Institute of Advanced Industrial Science and Technology (AIST), 1-1-1 Umezono, Tsukuba, Ibaraki 305-8568, Japan*
[3]*Institute for Solid State Physics, University of Tokyo, 5-1-5 Kashiwanoha, Kashiwa, Chiba 277-8581, Japan*
[4]*The Institute of Scientific and Industrial Research (ISIR), Osaka University, 8-1 Mihogaoka, Ibaraki, Osaka 567-0047, Japan*
(Received 27 July 2009; revised manuscript received 22 September 2009; published 14 October 2009)

When modeling a surface/interface using a slab geometry that imposes the periodic boundary condition, there are spurious dipole and higher-order multipole interactions with the image slabs. Here, we show that the effective screening medium (ESM) method [M. Otani and O. Sugino, Phys. Rev. B **73**, 115407 (2006)] can deal with such electrostatic issues rigorously in a slab calculation. After benchmark calculations for a hypothetical water layer, we show that there is an error in the total energy caused by the multipole interaction, but this can be treated efficiently using the ESM method. The accurate treatment of the electrostatic interaction is essential for performing large-scale surface/interface calculations.

DOI: 10.1103/PhysRevB.80.165411 PACS number(s): 73.20.−r, 68.35.Md, 31.15.E−

I. INTRODUCTION

Recent advances in computer technology and the development of efficient parallel algorithms[1–3] have enabled us to perform large-scale electronic structure calculations for solids. These calculations incorporate the use of highly optimized codes based on density functional theory (DFT).[4,5] With the DFT approach, the electronic structure is obtained by solving the Kohn-Sham equation, while the electrostatic interaction is dealt with by solving the Poisson equation. In conventional electronic structure codes wherein the plane-wave (PW) basis set and the pseudopotential frameworks are used, efficient Kohn-Sham solvers are available, such as the conjugate-gradient scheme,[6] the Davidson scheme,[7] or the residual vector minimization scheme–direct inversion in the iterative subspace (RMM-DIIS),[8–10] while an accurate solution of the Poisson equation is usually obtained using the fast Fourier transform (FFT).

Besides modeling solids, a large-scale surface/interface calculation is also possible by employing a slab model that is periodic in the surface lateral direction and nonperiodic in the surface normal direction. However, the use of the FFT implies the periodic boundary condition (PBC) on the system considered, resulting in the spurious electrostatic interaction of the slab with its periodic images, due to the long-range nature of the Coulomb potential. A natural way to resolve this is to use a real-space method,[11–17] accelerated by the multigrid technique[12,18–20] instead of the FFT. The multigrid approach has an advantage over the FFT-based one: it scales linearly with the number of the real-space grid point N, whereas the FFT scales as $N \log N$. The efficiency of both approaches is discussed in Ref. 20. Recently, Genovese *et al.*[21] developed a Poisson solver for surface problems using a scaling-interpolation function in the wavelet theory.

Despite the recent progress in real-space techniques, use of the FFT in conjunction with a PW basis set is well established and is still superior due to its simplicity and robustness. Indeed, several methods exist to correct the artificial electrostatic interaction in surface calculations within a PW framework. A popular method is the dipole correction,[22–24] in which a compensating dipole field is introduced to correct the artificial field across the slab. The spurious interaction removed by this scheme is still the dipole component, the lowest-order electrostatic interaction only.

It appears that the effect of the higher-order multipole interactions on the total energy has seldom been paid serious attention so far. Rather, the spurious interaction error has been somehow believed negligible when a slab has no net dipole moment. However, as the area of the surface considered becomes larger in a slab calculation, the higher-order multipole interaction should become significant. The purpose of this paper is to illustrate that the associated total-energy error can be intolerably large. We also show that this problem can be gotten rid of with a minimal modification of the FFT-based scheme instead of using more cumbersome real-space techniques.

For that purpose, one may use the Coulomb cutoff method[25–27] or the density-countercharge method,[28] in which the spurious interaction between the periodic images, including dipole and all higher-order multipole interactions, is eliminated. Meanwhile, use of a Green's function should provide a more sophisticated way. Indeed, the effective screening medium (ESM) method developed by Otani and Sugino[29] makes use of the facts that the Green's function is greatly simplified when the slab has a planar boundary condition and that the electrostatic potential is thereby obtained analytically. Then structure of the Poisson solver becomes very similar to that of the FFT-based one, and hence one needs minimal modification of the existing code. The ESM method is found not only as simple and stable as the FFT-based scheme but also enables flexible modeling of the surface using several BCs such as the Neumann and Cauchy, as well as the Dirichlet.

Below, we show that the ESM method can treat a slab with large multipole moments accurately within the FFT-based scheme without any "corrections." Efficiency of the

method is also demonstrated by comparing available methods. This capability is particularly important when performing large-scale surface/interface calculations, where accurate treatment of the electrostatic interaction is essential for obtaining an accurate total energy.

II. ESM METHOD

In this section, we briefly describe the ESM method since a more complete formulation was given elsewhere.[29] The free energy functional[30–33] is given as $F_{\mathrm{tot}}=E_{\mathrm{tot}}-\sigma S_{\mathrm{el}}$, where σ and S_{el} are the electronic temperature and entropy, respectively, and E_{tot} is the total energy given in terms of the Green's function $G(\boldsymbol{r},\boldsymbol{r}')$ of the Poisson equation by

$$E_{\mathrm{tot}}[\rho_{\mathrm{e}}] = T_{\mathrm{s}}[\rho_{\mathrm{e}}] + E_{\mathrm{xc}}[\rho_{\mathrm{e}}] + \int\int d\boldsymbol{r}d\boldsymbol{r}'\,\rho_{\mathrm{e}}(\boldsymbol{r})G(\boldsymbol{r},\boldsymbol{r}')\rho_{\mathrm{I}}(\boldsymbol{r}') + \frac{1}{2}\int\int d\boldsymbol{r}d\boldsymbol{r}'\,\rho_{\mathrm{e}}(\boldsymbol{r})G(\boldsymbol{r},\boldsymbol{r}')\rho_{\mathrm{e}}(\boldsymbol{r}') + \frac{1}{2}\int\int d\boldsymbol{r}d\boldsymbol{r}'\,\rho_{\mathrm{I}}(\boldsymbol{r})G(\boldsymbol{r},\boldsymbol{r}')\rho_{\mathrm{I}}(\boldsymbol{r}'), \tag{1}$$

where T_{s} and E_{xc} are one-particle kinetic and exchange-correlation energies, respectively. $\rho_{\mathrm{I}}(\boldsymbol{r})$ is the ionic charge density and the electronic charge density is given as $\rho_{\mathrm{e}}(\boldsymbol{r})=\Sigma_i f_i|\psi_i(\boldsymbol{r})|^2$, where f_i is the occupation number of the ith Kohn-Sham orbital $\psi_i(\boldsymbol{r})$. The third, fourth, and fifth terms denote the electron-ion interaction energy, the Hartree energy, and the ion-ion interaction energy, respectively. For a surface which is nonperiodic in the z direction, we consider the following Green's function in the Laue representation as

$$G^{\mathrm{b}}(\boldsymbol{g}_{\parallel},z,z') = \begin{cases} -2\pi|z-z'| & \text{if } g_{\parallel}=0 \\ \dfrac{2\pi}{g_{\parallel}}e^{-g_{\parallel}|z-z'|} & \text{if } g_{\parallel}\neq 0, \end{cases} \tag{2}$$

where $\boldsymbol{g}_{\parallel}$ is the two-dimensional reciprocal lattice vector, $g_{\parallel}$ is the absolute value of $\boldsymbol{g}_{\parallel}$, and $\boldsymbol{r}_{\parallel}$ is the real-space vector in the surface lateral direction. The divergent term in the $g_{\parallel}=0$ case is omitted for simplicity. Here, the superscript "b" is added to emphasize that the Green's function corresponds to the bare Coulomb interaction.

When the derivatives of the electrostatic potential are zero at infinity ($\pm\infty$), Eq. (1) is equivalent to the usual free energy functional within DFT. In addition to this boundary condition [the boundary condition (i) in Ref. 29] that we focus in this paper, one can use different boundary conditions within the ESM as well. On a slab sandwiched by two continuum media with the relative permittivity larger than unity, one can apply the Neumann and Caucy, as well as the Dirichlet; by this the computational scheme is called ESM.

The electrostatic potential is given by

$$V(\boldsymbol{g}_{\parallel},z) = \int dz'\,G^{\mathrm{b}}(\boldsymbol{g}_{\parallel},z,z')\rho(\boldsymbol{g}_{\parallel},z'), \tag{3}$$

where $\rho(\boldsymbol{g}_{\parallel},z')$ is the sum of the electronic and ionic charge densities. Using the fact that the wave functions and the charge density of the slab are confined to a certain region, i.e., within the supercell used, the integral appearing in Eq. (3) can be evaluated analytically without any approximation. Thus it is possible to calculate the exact electrostatic interaction energy with the ESM method and hence also the accurate total energy of the isolated slab and forces acting on the atoms. A detailed formulation is presented in Appendixes A and B.

TABLE I. Total energy of an H_2O molecule E_{tot}, that relative to the double cell ΔE and dipole moments μ, in a $0.3\times0.3\times1.2$ nm^3 unit cell, calculated using various approaches.

	E_{tot} (eV/H_2O)	ΔE (meV)	μ (D)
ESM	−471.233312	0.4	1.1314
Repeated slab	−471.286520	−52.8	1.2944
Dipole correction[a]	−471.186810	46.9	1.1316
Dipole correction[b]	−471.233306	0.4	1.1316
Double cell	−471.233730	0.0	

[a]Method of Neugebauer and Scheffler (Ref. 22).
[b]Method of Bengtsson (Ref. 23).

III. RESULTS AND DISCUSSION

The method presented here was implemented in a program package STATE.[34] In the following calculations, *ab initio* pseudopotentials[35,36] were used to represent the electron-ion interaction. A plane-wave basis set was used to expand the wave functions and the augmentation charge, with kinetic energy cutoffs of 25 and 225 Ry, respectively. The Perdew-Burke-Ernzerhof (PBE) exchange-correlation energy functional[37,38] was used throughout.

A. H_2O layer

We first performed the calculations on a water layer similar to the one used by Bengtsson[23] because the water molecule has a large dipole moment and is a good example for showing the effectiveness of the proposed method. A water molecule was placed in a tetragonal unit cell in such a way as to direct its dipole moment in the z direction. A $(6\times6\times1)$ uniform k-point mesh was then used to sample the Brillouin zone. We calculated the total energy and the dipole moment of the water molecule in a $0.3\times0.3\times1.2$ nm^3 unit cell using different approaches. As a reference, we compared the total energy to that of a doubled cell in the z direction, in which the water molecules are oriented in opposite directions. As a result, the net dipole moment is zero in the doubled cell. The results are presented in Table I.

Our results are similar to those described in an earlier report.[23] The reason for the difference in ΔE is the different choice of k-point mesh and unit cell size. The energy and dipole moment obtained using the ESM method are almost identical to those obtained by Bengtsson using the dipole correction. Note that the dipole correction relies on planar averages of the charge density and potential and is therefore only valid provided that the distance between the neighboring slabs is sufficiently larger than the lateral dimension. On

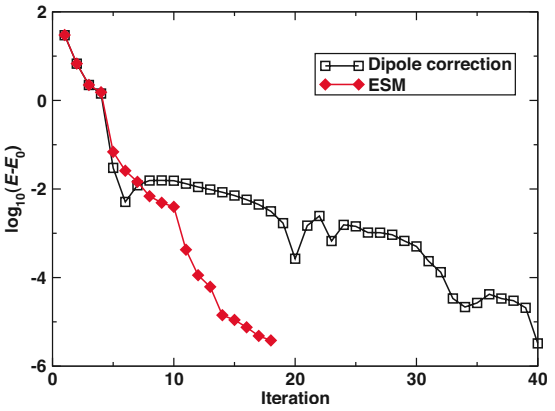

FIG. 1. (Color online) Convergence of the total energy (in eV) of the H_2O layer for the dipole correction and ESM methods. The values depicted are decimal logarithms of the difference between the total energy calculated at each self-consistency step (E) and the converged value (E_0).

the other hand, the ESM method yields the exact energy as long as the magnitude of the charge density in the vacuum region is negligibly small. Therefore, a smaller vacuum region can be chosen than that in the conventional approach, which is one of the advantages of the ESM method.

Here, it would be worthwhile to address the convergence issue[24] in the self-consistent cycle of the Kohn-Sham solver. In Fig. 1, we compare the convergence of the total energy using both the dipole correction and ESM methods. To ensure a fair comparison, we have used the same calculation conditions. The number of iterations with the ESM method is almost the same as that with the conventional approach without correction (not shown), whereas the convergence becomes very slow with the dipole correction method. The number of iterations necessary to reach the convergence is more than twice that in the present case. This is because the dipole correction tends to "overcorrect" the electrostatic potential of the system during the self-consistent cycle, leading to a charge-sloshing problem. Consequently it worsens the self-consistency. On the other hand, no such problem occurs with the ESM method and the convergence of the total energy is stable and robust.

B. NaCl sheet

To show the impact of the higher-order multipole interaction in the slab calculation, we consider a slab with a vanishing net dipole, which consists of polar molecules. It is expected that such a slab can be calculated accurately using the conventional PBC. The systems considered here are hypothetical sheets consisting of NaCl molecules with a large dipole moment.[39] We constructed the following two types of nonpolar NaCl sheets, as shown in Fig. 2. The first contains two NaCl molecules in a unit cell, with dipole moments opposite in the x direction (2×1), while in the other, the molecules are arrayed in such a way as to have alternating dipole moments every two molecules (4×4). The bond length of the NaCl molecule was fixed at the theoretical value (0.2382 nm), while the dimension of the surface unit cell was determined such that the intermolecular distances are larger than the sum of the van der Waals radii of Na and Cl atoms (0.227 nm for Na and 0.175 nm for Cl) to preserve the molecular nature of NaCl and the large dipole moment of the molecule. In practice, cell dimensions of 1.3×1.0 nm^2 for the (2×1) cell and 2.6×1.0 nm^2 for (4×1) were used. We calculated the total energy of the NaCl sheets as a function of the unit cell length in the surface normal direction L_z. In Fig. 3, the total energy relative to the converged value (total energy at $z=5$ nm) is plotted for both the PBC and ESM methods. Using the PBC, the errors in the total energy are 55 and 195 meV per unit cell at $z=1$ nm for the (2×1) and (4×1) cells, respectively, while the overlap between the charge densities of the neighboring cells is negligible. On the other hand, the ESM method gives the converged total energy at $z=1$ nm with the total energy showing almost no dependence on L_z. The results indicate that there is a possible error in the total energy using the PBC even when the slab has no net dipole moment and the charge density is negligibly small in the vacuum region.

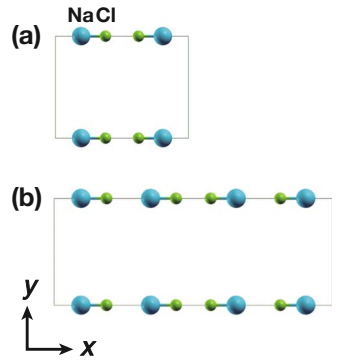

FIG. 2. (Color online) Hypothetical NaCl sheets used in the calculation: (a) (2×1) and (b) (4×1) unit cells.

To clarify the source of the error in the PBC calculation, we have plotted the electrostatic potentials in $\boldsymbol{g}_\parallel$ space [Eq.

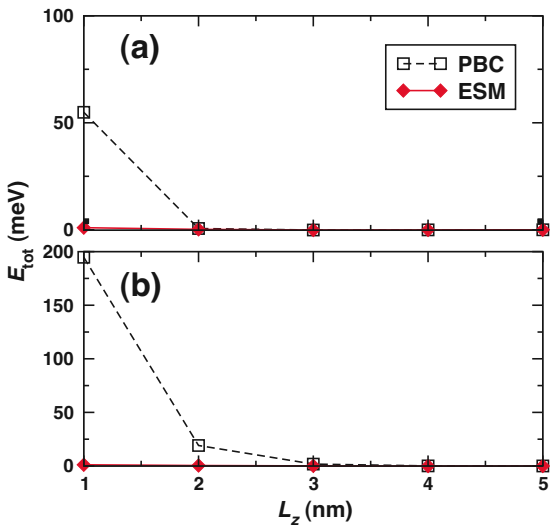

FIG. 3. (Color online) Total energy (per unit cell) as a function of the cell length in the direction normal to the surface (L_z) for (a) (2×1) and (b) (4×1) cells.

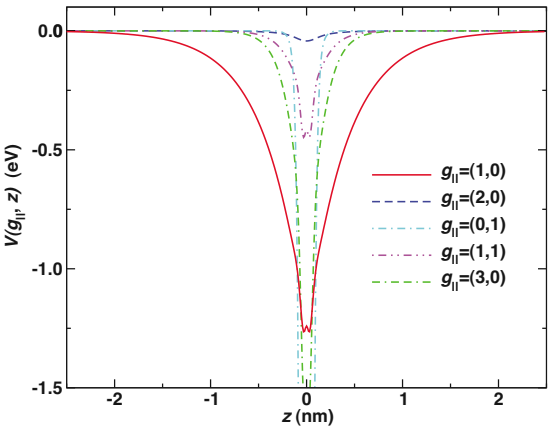

FIG. 4. (Color online) $\boldsymbol{g}_\parallel$ components of the electrostatic potential V for the (4×1) cell. $\boldsymbol{g}_\parallel$'s are expressed in terms of the basic reciprocal lattice vectors.

(3)]. Figure 4 shows some small $\boldsymbol{g}_\parallel \neq 0$ components of $V(\boldsymbol{g}_\parallel, z)$ for the (4×1) NaCl sheet located at $z=0$, which contribute to the higher-order multipole interaction. The $\boldsymbol{g}_\parallel = 0$ component, which contributes to the lowest electrostatic interaction of the dipole interaction, is not shown. We found that the smallest $\boldsymbol{g}_\parallel \neq 0$ component $[\boldsymbol{g}_\parallel=(1,0)]$, corresponding to the quadrupole interaction, decays very slowly and the potential remains finite ($\sim$3 meV) even at the large distance of $z=\pm 2.5$ nm from the sheet. The next smallest component of $\boldsymbol{g}_\parallel=(2,0)$ becomes negligible (less than 1 meV) at 0.75 nm, while larger $g_\parallel$ components decay much more rapidly. The plot indicates that there are contributions from the higher-order multipole interaction. Small $\boldsymbol{g}_\parallel \neq 0$ components of $V(\boldsymbol{g}_\parallel, z)$ extend spatially and overlap with the charge densities of the neighboring slab in the PBC calculation, resulting in a non-negligible error in the total energy with a relatively small L_z. This explains the error in the total energy at small L_z values. On the other hand, the ESM method imposes no periodic boundary condition in the z direction. There is, therefore, no overlap between the higher-order electrostatic potential and the charge density of the neighboring slab. Thus, no error is found in the ESM total-energy calculations, provided that the magnitude of the charge density in the vacuum region is negligibly small. Note that errors also exist in the Hellmann-Feynman forces using the PBC as well as the total energy: the maximum errors are 0.03 and 0.14 nN in the (2×1) and (4×1) cells, respectively (1 nN $=0.0121$ hartree/bohr).

In principle, the error due to the spurious electrostatic interaction in a PBC calculation can be minimized by increasing the vacuum region. However, such a convergence check becomes much more demanding as the system size increases. Moreover, the effect of the higher-order multipole interaction becomes larger as the system size increases. As demonstrated above, the ESM method gives the converged total energy of a slab with the smallest vacuum region. It is a great advantage especially in a large-scale calculation, as the method can reduce the necessary vacuum region, and hence the computational cost, without sacrificing the accuracy of the calculation.

IV. SUMMARY

In summary, we have shown that in addition to the well-known dipole-dipole interaction, there is a possible error due to the higher-order multipole interaction in a periodic slab calculation, but such errors can be eliminated by using the ESM method. Furthermore, the convergence problem rarely occurs in the ESM method unlike in the dipole correction, making the method very efficient for slab calculations. We have also shown that it is possible to minimize the vacuum region required in slab calculations, without sacrificing the accuracy of the total energy and forces. This is an important advantage compared with the Coulomb cutoff method: the method requires the supercell size at least twice as the slab thickness.[42] Finally, we note that although the implementation of the ESM method presented here is specific to the plane-wave pseudopotential framework, it is applicable to any electronic structure code by modifying the modules related to the electrostatic (Hartree) potential and energy.[43] The ESM method should be the method of choice for studying *any* surface or interface within the slab approach.

ACKNOWLEDGMENTS

This work was partly supported by a Grant-in-Aid for Scientific Research in Priority Areas (Development of New Quantum Simulations and Quantum Designs, Grant No. 1706400) from the Ministry of Education, Culture, Sports, Science and Technology, Japan. Numerical calculations were performed at the Cybermedia Center, Osaka University, at the Supercomputer Center, Institute for Solid State Physics, University of Tokyo, at the Information Technology Center, University of Tokyo, and at the Cyberscience Center, Tohoku University.

APPENDIX A: ION-ION INTERACTION, LOCAL POTENTIAL, AND HARTREE POTENTIAL ENERGY

In this appendix, we present the detailed expressions for the total energy within the plane-wave pseudopotential framework, as used in the practical implementation. We use the same notations as given in the original paper by Otani and Sugino.[29]

The ion-ion contribution to the total energy, $E_{\rm ion}$, per whole slab in the ESM method is given as

$$E_{\rm ion} = \sum_{\boldsymbol{R}_\parallel \boldsymbol{R}'_\parallel} \sum_{\mu\nu} \frac{Z_\mu Z_\nu}{2} \int\int d\boldsymbol{r} d\boldsymbol{r}'\, \delta(\boldsymbol{r} - \boldsymbol{R}_{\parallel\mu}) \times G^{\rm b}(\boldsymbol{r}_\parallel - \boldsymbol{r}'_\parallel, z, z')\, \delta(\boldsymbol{r}' - \boldsymbol{R}'_{\parallel\nu}) - E_{\rm self}, \quad \text{(A1)}$$

where Z_μ is the ionic charge of the μth ion and $\boldsymbol{R}_{\parallel\mu}$ is shorthand notation for the atomic position $\boldsymbol{\tau}_\mu$ in a unit cell labeled by $\boldsymbol{R}_\parallel$. The last term is the self-interaction energy defined as

$$E_{\rm self} = \sum_{\boldsymbol{R}_\parallel} \sum_{\mu} \frac{Z_\mu^2}{2} \int\int d\boldsymbol{r} d\boldsymbol{r}'\, \delta(\boldsymbol{r} - \boldsymbol{R}_{\parallel\mu}) \times G^{\rm b}(\boldsymbol{r}_\parallel - \boldsymbol{r}'_\parallel, z, z')\, \delta(\boldsymbol{r}' - \boldsymbol{R}'_{\parallel\nu}). \quad \text{(A2)}$$

By introducing a fictitious Gaussian charge

$$\rho_{\mathrm{fic}}(\boldsymbol{r}-\boldsymbol{R}_{\parallel\mu})=\frac{Z_\mu\eta^3}{\pi^{3/2}}e^{-\eta^2|\boldsymbol{r}-\boldsymbol{R}_{\parallel\mu}|^2}, \tag{A3}$$

the first term of Eq. (A1) can be split into a long-range part $E_{\mathrm{ion}}^{\mathrm{LR}}$ and a short-range part $E_{\mathrm{ion}}^{\mathrm{SR}}$ as

$$E_{\mathrm{ion}}^{\mathrm{LR}}=\sum_{\boldsymbol{R}_\parallel\boldsymbol{R}'_\parallel}\sum_{\mu\nu}\frac{Z_\mu}{2}\int\int d\boldsymbol{r}d\boldsymbol{r}'\,\delta(\boldsymbol{r}-\boldsymbol{R}_{\parallel\mu})\times G^{\mathrm{b}}(\boldsymbol{r}_\parallel-\boldsymbol{r}'_\parallel,z,z')\rho_{\mathrm{fic}}(\boldsymbol{r}'-\boldsymbol{R}'_{\parallel\nu}) \tag{A4}$$

and

$$E_{\mathrm{ion}}^{\mathrm{SR}}=\sum_{\boldsymbol{R}_\parallel\boldsymbol{R}'_\parallel}\sum_{\mu\nu}\frac{Z_\mu}{2}\int\int d\boldsymbol{r}d\boldsymbol{r}'\,\delta(\boldsymbol{r}-\boldsymbol{R}_{\parallel\mu})\times G^{\mathrm{b}}(\boldsymbol{r}_\parallel-\boldsymbol{r}'_\parallel,z,z')[Z_\nu\delta(\boldsymbol{r}'-\boldsymbol{R}'_{\parallel\nu})-\rho_{\mathrm{fic}}(\boldsymbol{r}'-\boldsymbol{R}'_{\parallel\nu})]. \tag{A5}$$

Although Eqs. (B4) and (B5) in the original paper[29] were incorrect, the final expression was unaffected. The corresponding correct expressions are given by Eqs. (A4) and (A5), respectively. Furthermore, η is chosen to ensure good convergence of both real and reciprocal space summations. After some algebraic manipulation, the following expression is obtained for the ion-ion interaction per unit cell:

$$\begin{aligned}E_{\mathrm{ion}}=&\sum_{\boldsymbol{R}_\parallel}\sum_{\mu\nu}\frac{Z_\mu Z_\nu}{2}\frac{\mathrm{erfc}(\eta|\boldsymbol{R}_{\parallel\mu}-\boldsymbol{\tau}_\nu|)}{|\boldsymbol{R}_{\parallel\mu}-\boldsymbol{\tau}_\nu|}-\sum_\mu Z_\mu^2\frac{\eta}{\sqrt{\pi}}\\&+\sum_{\boldsymbol{g}_\parallel\neq0}\sum_{\mu\nu}\frac{Z_\mu Z_\nu}{2S_0}e^{i\boldsymbol{g}_\parallel\cdot(\boldsymbol{\tau}_{\mu\parallel}-\boldsymbol{\tau}_{\nu\parallel})}F_1^\eta(\boldsymbol{g}_\parallel,\tau_\mu^z,\tau_\nu^z)\\&-\sum_{\mu\nu}\frac{\pi Z_\mu Z_\nu}{S_0}\left[(\tau_\mu^z-\tau_\nu^z)\mathrm{erf}[\eta(\tau_\mu^z-\tau_\nu^z)]\right.\\&\left.+\frac{1}{\eta\sqrt{\pi}}e^{-\eta^2(\tau_\mu^z-\tau_\nu^z)^2}\right],\end{aligned} \tag{A6}$$

where S_0 is the area of the surface unit cell, $\boldsymbol{\tau}_{\mu\parallel}$ (τ_μ^z) are surface parallel (normal) components of atomic position, $\mathrm{erf}(x)=2/\sqrt{\pi}\int_0^x dte^{-t^2}$ and $\mathrm{erfc}(x)=1-\mathrm{erf}(x)$ are the error function and complementary error function, respectively, and F_1^η is defined as

$$F_1^\eta(\boldsymbol{g}_\parallel,z,z')=\frac{\pi}{g_\parallel}\left\{e^{-g_\parallel(z-z')}\,\mathrm{erfc}\left[\frac{g_\parallel}{2\eta}-\eta(z-z')\right]+e^{g_\parallel(z-z')}\,\mathrm{erfc}\left[\frac{g_\parallel}{2\eta}+\eta(z-z')\right]\right\}. \tag{A7}$$

The sum over $\boldsymbol{R}_\parallel$ appearing in the first term of Eq. (A6) excludes $\boldsymbol{R}_{\parallel\mu}-\boldsymbol{\tau}_\nu=0$.

The electron-ion interaction energy $E_{\mathrm{e\text{-}i}}$ in the pseudopotential method is divided into three parts as follows:

$$E_{\mathrm{e\text{-}i}}=\int d\boldsymbol{r}V_{\mathrm{loc}}^{\mathrm{LR}}(\boldsymbol{r})\rho_{\mathrm{e}}(\boldsymbol{r})+\int d\boldsymbol{r}V_{\mathrm{loc}}^{\mathrm{SR}}(\boldsymbol{r})\rho_{\mathrm{e}}(\boldsymbol{r})+\sum_i f_i\langle\psi_i|V_{\mathrm{NL}}|\psi_i\rangle, \tag{A8}$$

where the first and second terms are the long-range and short-range parts of the local potential energy, respectively, while the third term represents the nonlocal potential energy. The latter two terms are calculated as in the conventional approach.

The long-range part of the local potential originates from the core charge mimicked by the superposition of the Gaussian functions centered at the atomic sites,[45]

$$\rho_{\mathrm{g}}(\boldsymbol{r}_\parallel,z)=\sum_{\boldsymbol{R}_\parallel}\sum_\mu\rho_\mu(\boldsymbol{r}_\parallel-\boldsymbol{R}_{\parallel\mu},z-\tau_\mu^z), \tag{A9}$$

where

$$\rho_\mu(\boldsymbol{r})=\sum_j^{N_{\mathrm{Gaussian}}}\frac{Z_\mu\beta_j^\mu(\alpha_j^\mu)^2}{\pi^{3/2}}e^{-(\alpha_j^\mu)^2|\boldsymbol{r}|^2}. \tag{A10}$$

Here $\Sigma_j^{N_{\mathrm{Gaussian}}}\beta_j^\mu=1$ and α_j^μ is a decay constant for the Gaussian function. In addition, N_{Gaussian} denotes the number of Gaussian functions, which is two in the present implementation. The local potential in $\boldsymbol{g}_\parallel$ space is calculated as

$$V_{\mathrm{loc}}^{\mathrm{LR}}(\boldsymbol{g}_\parallel,z)=\int_{-\infty}^{\infty}dz'G^{\mathrm{b}}(\boldsymbol{g}_\parallel,z,z')\rho_{\mathrm{g}}(\boldsymbol{g}_\parallel,z'), \tag{A11}$$

which leads to the following expressions:

$$V_{\mathrm{loc}}^{\mathrm{LR}}(\boldsymbol{g}_\parallel\neq0,z)=\sum_\mu\frac{Z_\mu}{S_0}e^{-i\boldsymbol{g}_\parallel\cdot\boldsymbol{\tau}_{\mu\parallel}}\sum_j^{N_{\mathrm{Gaussian}}}\beta_j^\mu F_1^{\alpha_j^\mu}(\boldsymbol{g}_\parallel,z,\tau_\mu^z) \tag{A12}$$

and

$$V_{\mathrm{loc}}^{\mathrm{LR}}(\boldsymbol{g}_\parallel=0,z)=-\sum_\mu\frac{2\pi Z_\mu}{S_0}\sum_j^{N_{\mathrm{Gaussian}}}\beta_j^\mu\times\left[(z-\tau_\mu^z)\mathrm{erf}[\alpha_j^\mu(z-\tau_\mu^z)]+\frac{1}{\alpha_j^\mu\sqrt{\pi}}e^{-(\alpha_j^\mu)^2(z-\tau_\mu^z)^2}\right]. \tag{A13}$$

The divergent term in $V_{\mathrm{loc}}^{\mathrm{LR}}(\boldsymbol{g}_\parallel=0,z)$ is discarded because it is canceled together with that in the Hartree potential. Similar expressions for the local potential and ion-ion interaction energy are given in Ref. 46.

The Hartree potential V_{H} in $\boldsymbol{g}_\parallel$ space is calculated as

$$V_{\mathrm{H}}(\boldsymbol{g}_\parallel,z)=\int dz'G^{\mathrm{b}}(\boldsymbol{g}_\parallel,z,z')\rho_{\mathrm{e}}(\boldsymbol{g}_\parallel,z')=\int_{-z_0}^{z_0}dz'G^{\mathrm{b}}(\boldsymbol{g}_\parallel,z,z')\rho_{\mathrm{e}}(\boldsymbol{g}_\parallel,z'), \tag{A14}$$

where we define the unit cell in the z direction as spanned in the region $[-z_0,z_0]$ and assume that the electronic charge density $\rho_{\mathrm{e}}(\boldsymbol{r})$ is localized so that the overlap of the wave functions in the vacuum region is negligible. By virtue of the

localized nature of the charge density, we can use the Fourier transform in the z direction as

$$\rho_{\mathrm{e}}(\boldsymbol{g}_{\parallel},z)=\sum_{g_{\parallel}}\rho_{\mathrm{e}}(\boldsymbol{g}_{\parallel},g_z)e^{ig_z z}. \tag{A15}$$

After tedious yet straightforward calculations, we obtain the final expressions for the Hartree potential as

$$\begin{aligned}V_{\mathrm{H}}(\boldsymbol{g}_{\parallel}\neq 0,z)&=4\pi\sum_{g_z}\frac{\rho_{\mathrm{e}}(\boldsymbol{g}_{\parallel},g_z)}{g_{\parallel}^2+g_z^2}e^{ig_z z}-2\pi\frac{e^{-g_{\parallel}(z+z_0)}}{g_{\parallel}}\sum_{g_z}\frac{\rho_{\mathrm{e}}(\boldsymbol{g}_{\parallel},g_z)}{g_{\parallel}+ig_z}e^{-ig_z z_0}\\&\quad-2\pi\frac{e^{g_{\parallel}(z-z_0)}}{g_{\parallel}}\sum_{g_z}\frac{\rho_{\mathrm{e}}(\boldsymbol{g}_{\parallel},g_z)}{g_{\parallel}-ig_z}e^{ig_z z_0}\end{aligned} \tag{A16}$$

and

$$\begin{aligned}V_{\mathrm{H}}(\boldsymbol{g}_{\parallel}=0,z)&=4\pi\sum_{g_z\neq 0}\frac{\rho_{\mathrm{e}}(\boldsymbol{g}_{\parallel}=0,g_z)}{g_z^2}e^{ig_z z}\\&\quad-2\pi i(z-z_0)\sum_{g_z\neq 0}\frac{\rho_{\mathrm{e}}(\boldsymbol{g}_{\parallel}=0,g_z)}{g_z}e^{ig_z z_0}\\&\quad-2\pi i(z+z_0)\sum_{g_z\neq 0}\frac{\rho_{\mathrm{e}}(\boldsymbol{g}_{\parallel}=0,g_z)}{g_z}e^{-ig_z z_0}\\&\quad-4\pi\sum_{g_z\neq 0}\frac{\rho(\boldsymbol{g}_{\parallel}=0,g_z)}{g_z^2}\cos(g_z z_0)\\&\quad-2\pi(z^2+z_0^2)\rho_{\mathrm{e}}(\boldsymbol{g}_{\parallel}=0,g_z=0).\end{aligned} \tag{A17}$$

The divergent term is once again omitted as explained above. Finally, the Hartree energy E_{H} is calculated in real space as

$$E_{\mathrm{H}}=\frac{1}{2}\int d\boldsymbol{r}V_{\mathrm{H}}(\boldsymbol{r})\rho_{\mathrm{e}}(\boldsymbol{r}). \tag{A18}$$

APPENDIX B: DERIVATIVES OF ION-ION INTERACTION ENERGY AND LOCAL POTENTIAL

Because the present method obeys the variational principle, i.e., the ground state is obtained by minimizing the total-energy functional (or the free energy when electronic temperature is introduced), the Hellmann-Feynman forces are calculated as in the conventional method. In the ESM method, the Hellmann-Feynman forces are calculated analytically along with the total energy. The force acting on the μth atom in the α direction (α=x,y,z) with norm-conserving pseudopotentials is calculated as

$$\begin{aligned}F_{\mu}^{\alpha}&=-\frac{\partial F_{\mathrm{tot}}}{\partial\tau_{\mu}^{\alpha}}\\&=-\int d\boldsymbol{r}\frac{\partial V_{\mathrm{loc}}^{\mathrm{LR}}(\boldsymbol{r})}{\partial\tau_{\mu}^{\alpha}}\rho_{\mathrm{e}}(\boldsymbol{r})-\int d\boldsymbol{r}\frac{\partial V_{\mathrm{loc}}^{\mathrm{SR}}(\boldsymbol{r})}{\partial\tau_{\mu}^{\alpha}}\rho_{\mathrm{e}}(\boldsymbol{r})\\&\quad-\sum_i f_i\langle\psi_i|\frac{\partial V_{\mathrm{NL}}}{\partial\tau_{\mu}^{\alpha}}|\psi_i\rangle-\frac{\partial E_{\mathrm{ion}}}{\partial\tau_{\mu}^{\alpha}},\end{aligned} \tag{B1}$$

where τ_{μ}^{α} is the α component of the atomic coordinate, $V_{\mathrm{loc}}^{\mathrm{LR}}(\boldsymbol{r})$ and $V_{\mathrm{loc}}^{\mathrm{SR}}(\boldsymbol{r})$ are long-range and short-range parts of the local potential, respectively, and V_{NL} is the nonlocal pseudopotential. $V_{\mathrm{loc}}^{\mathrm{LR}}(\boldsymbol{r})$ originates from the effective core charge $\rho_{\mathrm{g}}(\boldsymbol{r})$ and $V_{\mathrm{loc}}^{\mathrm{SR}}(\boldsymbol{r})$ is obtained by extracting $V_{\mathrm{loc}}^{\mathrm{LR}}(\boldsymbol{r})$ from the local potential obtained from the atomic calculation. The sole difference from the conventional plane-wave pseudopotential method is the treatment of the long-range component of the local potential and the ion-ion interaction energy. These derivatives are modified accordingly. Furthermore, other terms [$V_{\mathrm{loc}}^{\mathrm{SR}}(\boldsymbol{r})$ and V_{NL}] are calculated exactly as in the conventional approach.

The contribution from the ion-ion interaction is

$$\begin{aligned}\frac{\partial E_{\mathrm{ion}}}{\partial\tau_{\mu}^{\alpha}}&=\sum_{\boldsymbol{G}_{\parallel}}\sum_{\mu}Z_{\nu}Z_{\mu}\left[\frac{2\eta}{\sqrt{\pi}}\frac{R_{\parallel}^{\alpha}+\tau_{\mu}^{\alpha}-\tau_{\nu}^{\alpha}}{|\boldsymbol{R}_{\parallel}+\boldsymbol{\tau}_{\mu}-\boldsymbol{\tau}_{\nu}|}e^{\eta^2|\boldsymbol{R}_{\parallel}+\boldsymbol{\tau}_{\mu}-\boldsymbol{\tau}_{\nu}|^2}\right.\\&\quad\left.-\frac{R_{\parallel}^{\alpha}+\tau_{\mu}^{\alpha}-\tau_{\nu}^{\alpha}}{|\boldsymbol{R}_{\parallel}+\boldsymbol{\tau}_{\mu}-\boldsymbol{\tau}_{\nu}|^3}\mathrm{erf}(\eta^2|\boldsymbol{R}_{\parallel}+\boldsymbol{\tau}_{\mu}-\boldsymbol{\tau}_{\nu}|^2)\right]\\&\quad+\sum_{\nu}\frac{Z_{\mu}Z_{\nu}}{S_0}\sum_{\boldsymbol{g}_{\parallel}\neq 0}g_{\parallel}^{\alpha}\sin[\boldsymbol{g}_{\parallel}\cdot(\boldsymbol{\tau}_{\mu\parallel}-\boldsymbol{\tau}_{\nu\parallel})]\\&\quad\times F_1^{\eta}(\boldsymbol{g}_{\parallel},\tau_{\mu}^{z},\tau_{\nu}^{z})(1-\delta_{\alpha,z})\\&\quad+\sum_{\nu}\frac{Z_{\mu}Z_{\nu}}{S_0}\sum_{\boldsymbol{g}_{\parallel}\neq 0}e^{-i\boldsymbol{g}_{\parallel}\cdot(\boldsymbol{\tau}_{\mu\parallel}-\boldsymbol{\tau}_{\nu\parallel})}G_1^{\eta}(\boldsymbol{g}_{\parallel},\tau_{\mu}^{z},\tau_{\nu}^{z})\delta_{\alpha,z}\\&\quad+\sum_{\nu}\frac{2\pi Z_{\mu}Z_{\nu}}{S_0}\mathrm{erf}[\eta(\tau_{\mu}^{z}-\tau_{\nu}^{z})]\delta_{\alpha,z},\end{aligned} \tag{B2}$$

where $g_{\parallel}^{\alpha}$ is the α component of the two-dimensional reciprocal lattice vector $\boldsymbol{g}_{\parallel}$ and

$$\begin{aligned}G_1^{\eta}(\boldsymbol{g}_{\parallel},z,z')&=\pi e^{-g_{\parallel}(z-z')}\,\mathrm{erfc}\left[\frac{g_{\parallel}}{2\eta}-\eta(z-z')\right]\\&\quad-\pi e^{g_{\parallel}(z-z')}\,\mathrm{erfc}\left[\frac{g_{\parallel}}{2\eta}+\eta(z-z')\right].\end{aligned} \tag{B3}$$

The derivative of $V_{\mathrm{loc}}^{\mathrm{LR}}$ with respect to the atomic position is calculated as

$$\begin{aligned}&\frac{\partial}{\partial\tau_{\mu}^{\alpha}}V_{\mathrm{loc}}^{\mathrm{LR}}(\boldsymbol{g}_{\parallel}\neq 0,z)\\&=\frac{Z_{\mu}}{S_0}e^{-i\boldsymbol{g}_{\parallel}\cdot\boldsymbol{\tau}_{\mu\parallel}}\sum_{j}^{N_{\mathrm{Gaussian}}}b_j^{\mu}[(-ig_{\parallel}^{\alpha})F_1^{\alpha_j^{\mu}}(\boldsymbol{g}_{\parallel},z,\tau_{\mu}^{z})(1-\delta_{\alpha,z})\\&\quad+G_1^{\alpha_j^{\mu}}(\boldsymbol{g}_{\parallel},z,\tau_{\mu}^{z})\delta_{\alpha,z}]\end{aligned} \tag{B4}$$

and

$$\frac{\partial}{\partial\tau_{\mu}^{\alpha}}V_{\mathrm{loc}}^{\mathrm{LR}}(\boldsymbol{g}_{\parallel}=0,z)=\frac{2\pi Z_{\mu}}{S_0}\sum_{j}^{N_{\mathrm{Gaussian}}}b_j^{\mu}\,\mathrm{erf}[a_j^{\mu}(z-\tau_{\mu}^{z})]\delta_{\alpha,z}. \tag{B5}$$

*ikutaro@wpi-aimr.tohoku.ac.jp

[1] J. Hutter and A. Curioni, Parallel Comput. **31**, 1 (2005).
[2] J. Hutter and A. Curioni, ChemPhysChem **6**, 1788 (2005).
[3] F. Gygi, IBM J. Res. Dev. **52**, 137 (2008).
[4] P. Hohenberg and W. Kohn, Phys. Rev. **136**, B864 (1964).
[5] W. Kohn and L. J. Sham, Phys. Rev. **140**, A1133 (1965).
[6] W. H. Press, B. P. Flannery, S. A. Teukolsky, and W. T. Vetterling, *Numerical Recipes* (Cambridge University Press, New York, 1986).
[7] E. R. Davidson, J. Comput. Phys. **17**, 87 (1975).
[8] P. Pulay, Chem. Phys. Lett. **73**, 393 (1980).
[9] D. M. Wood and A. Zunger, J. Phys. A **18**, 1343 (1985).
[10] G. Kresse and J. Furthmüller, Phys. Rev. B **54**, 11169 (1996).
[11] J. R. Chelikowsky, N. Troullier, and Y. Saad, Phys. Rev. Lett. **72**, 1240 (1994).
[12] E. L. Briggs, D. J. Sullivan, and J. Bernholc, Phys. Rev. B **52**, R5471 (1995).
[13] S. Goedecker, Rev. Mod. Phys. **71**, 1085 (1999).
[14] T. L. Beck, Rev. Mod. Phys. **72**, 1041 (2000).
[15] K. Varga, Z. Zhang, and S. T. Pantelides, Phys. Rev. Lett. **93**, 176403 (2004).
[16] K. Hirose, T. Ono, Y. Fujimoto, and S. Tsukamoto, *First-Principles Calculations in Real-Space Formalism: Electronic Configurations and Transport Properties of Nanostructures* (Imperial College Press, London, 2005).
[17] A. Natan, A. Benjamini, D. Naveh, L. Kronik, M. L. Tiago, S. P. Beckman, and J. R. Chelikowsky, Phys. Rev. B **78**, 075109 (2008).
[18] W. L. Briggs, V. E. Henson, and S. F. McCormick, *A Multigrid Tutorial* (SIAM, Philadelphia, 2000).
[19] E. Tsuchida and M. Tsukada, J. Phys. Soc. Jpn. **67**, 3844 (1998).
[20] E. Artacho *et al.*, J. Phys.: Condens. Matter **20**, 064208 (2008).
[21] L. Genovese, T. Deutsch, and S. Goedecker, J. Chem. Phys. **127**, 054704 (2007).
[22] J. Neugebauer and M. Scheffler, Phys. Rev. B **46**, 16067 (1992).
[23] L. Bengtsson, Phys. Rev. B **59**, 12301 (1999).
[24] A. Natan, L. Kronik, and Y. Shapira, Appl. Surf. Sci. **252**, 7608 (2006).
[25] The Coulomb cutoff technique has been applied to the calculations of finite systems. The first application of the method to a surface problem was done by J. J. Mortensen and M. Parrinello, J. Phys. Chem. B **104**, 2901 (2000), see footnote 23 therein.
[26] C. A. Rozzi, D. Varsano, A. Marini, E. K. U. Gross, and A. Rubio, Phys. Rev. B **73**, 205119 (2006).
[27] P. Mináry, M. E. Tuckerman, K. A. Pihakari, and G. J. Martyna, J. Chem. Phys. **116**, 5351 (2002).
[28] I. Dabo, B. Kozinsky, N. E. Singh-Miller, and N. Marzari, Phys. Rev. B **77**, 115139 (2008).
[29] M. Otani and O. Sugino, Phys. Rev. B **73**, 115407 (2006).
[30] N. D. Mermin, Phys. Rev. **137**, A1441 (1965).
[31] R. M. Wentzcovitch, J. L. Martins, and P. B. Allen, Phys. Rev. B **45**, 11372 (1992).
[32] M. Weinert and J. W. Davenport, Phys. Rev. B **45**, 13709 (1992).
[33] T. Oda, J. Phys. Soc. Jpn. **71**, 519 (2002).
[34] Y. Morikawa, Phys. Rev. B **51**, 14802 (1995).
[35] D. Vanderbilt, Phys. Rev. B **41**, 7892 (1990).
[36] N. Troullier and J. L. Martins, Phys. Rev. B **43**, 1993 (1991).
[37] J. P. Perdew, K. Burke, and M. Ernzerhof, Phys. Rev. Lett. **77**, 3865 (1996).
[38] J. P. Perdew, K. Burke, and M. Ernzerhof, Phys. Rev. Lett. **78**, 1396 (1997).
[39] The experimental value is 9.00 D (Ref. 40). Our PBE value is 8.32 D at the optimized bond length of 0.2382 nm, which is smaller than the experimental value of 9.00 D, while it is close to the local-density approximation value of 8.2 D (Ref. 41).
[40] *CRC Handbook of Chemistry and Physics*, 89th ed. (CRC, Boca Raton, FL, 2008).
[41] M. R. Jarvis, I. D. White, R. W. Godby, and M. C. Payne, Phys. Rev. B **56**, 14972 (1997).
[42] L. Yu, V. Ranjan, W. Lu, J. Bernholc, and M. Buongiorno Nardelli, Phys. Rev. B **77**, 245102 (2008).
[43] See the implementation on the SIESTA (Ref. 44) pseudoatomic orbital code, http://sugino.issp.u-tokyo.ac.jp/esm/
[44] J. Soler, E. Artacho, J. D. Gale, A. García, J. Junquera, P. Ordejón, and D. Sánchez-Portal, J. Phys.: Condens. Matter **14**, 2745 (2002).
[45] G. B. Bachelet, D. R. Hamann, and M. Schlüter, Phys. Rev. B **26**, 4199 (1982).
[46] T. Ono and K. Hirose, Phys. Rev. B **72**, 085105 (2005).